Boundary-Layer Meteorol (2018) 169:139–150
https://doi.org/10.1007/s10546-018-0354-6

NOTES AND COMMENTS

Boundary Conditions for Scalar (Co)Variances over Heterogeneous Surfaces

Ekaterina Machulskaya[1] · **Dmitrii Mironov**[1]

Received: 4 October 2017 / Accepted: 5 May 2018 / Published online: 31 May 2018

Abstract The problem of boundary conditions for the variances and covariances of scalar quantities (e.g., temperature and humidity) at the underlying surface is considered. If the surface is treated as horizontally homogeneous, Monin–Obukhov similarity suggests the Neumann boundary conditions that set the surface fluxes of scalar variances and covariances to zero. Over heterogeneous surfaces, these boundary conditions are not a viable choice since the spatial variability of various surface and soil characteristics, such as the ground fluxes of heat and moisture and the surface radiation balance, is not accounted for. Boundary conditions are developed that are consistent with the tile approach used to compute scalar (and momentum) fluxes over heterogeneous surfaces. To this end, the third-order transport terms (fluxes of variances) are examined analytically using a triple decomposition of fluctuating velocity and scalars into the grid-box mean, the fluctuation of tile-mean quantity about the grid-box mean, and the sub-tile fluctuation. The effect of the proposed boundary conditions on mixing in an archetypical stably-stratified boundary layer is illustrated with a single-column numerical experiment. The proposed boundary conditions should be applied in atmospheric models that utilize turbulence parametrization schemes with transport equations for scalar variances and covariances including the third-order turbulent transport (diffusion) terms.

Keywords Scalar variances and covariances · Surface boundary conditions · Tile approach · Turbulence parametrization scheme

1 Introduction

Advanced turbulence parametrization schemes that carry transport equations (with due regard for the third-order turbulent transport terms) not only for the turbulence kinetic energy (TKE)

✉ Ekaterina Machulskaya
ekaterina.machulskaya@dwd.de

Dmitrii Mironov
dmitrii.mironov@dwd.de

[1] Deutscher Wetterdienst, FE14, Frankfurter Str. 135, 63067 Offenbach am Main, Germany

but also for the variances and covariances of scalar quantities (e.g., temperature and humidity) attract increasing attention in geophysical applications, including numerical weather prediction (NWP) and climate modelling. The schemes developed by Mellor and Yamada (1974, their level-3 closure), Kenjereš and Hanjalić (2002), Nakanishi and Niino (2004), and Mironov and Machulskaya (2017) are such examples. These schemes are advantageous in many respects over one-equation TKE schemes and over more simple algebraic schemes. Recall that one-equation schemes utilize the transport equation for the TKE, whereas all other second-moment equations (i.e., the equations for the Reynolds stress and for the fluxes, variances and covariances of scalar quantities) are reduced to diagnostic expressions by neglecting the time-rate-of-change, advection, and third-order transport terms. Within the framework of the algebraic schemes, all second-moment equations, including the TKE equation, are truncated to the diagnostic expressions. It is worth noting that the simplified treatment of scalar (co)variances leads to down-gradient formulations of scalar fluxes, although the scalar (co)variances per se may not be used explicitly by the host atmospheric model. Apart from a consistent handling of counter-gradient fluxes of scalars (see discussion in Mironov 2009) the advantages of turbulence schemes with the scalar (co)variance transport equations include a more coherent treatment of kinetic and potential energy of the flow, and an improved representation of fractional cloudiness within the framework of statistical cloud schemes (Machulskaya and Mironov 2013).

Transport equations for the scalar variances and covariances require appropriate boundary conditions at the underlying surface. The present contribution addresses the problem of setting boundary conditions for scalar (co)variances at heterogeneous surfaces. A proper account of the surface heterogeneity effects, including physically-sound boundary conditions, is crucial for describing various important features of atmospheric flows. Secondary circulations in the convective boundary layer (e.g., Lynn et al. 1995) and enhanced vertical mixing in the stably-stratified boundary layer over heterogeneous surfaces (e.g., Stoll and Porté-Agel 2009; Mironov and Sullivan 2016) are illustrative examples.

If the grid-box of an atmospheric model adjacent to the underlying surface is treated as horizontally homogeneous (although it may be heterogeneous in reality), the Neumann boundary conditions that set the surface fluxes of scalar (co)variances to zero are appropriate. These boundary conditions are compatible with the surface-layer Monin–Obukhov similarity relationships. If, however, the surface heterogeneity is taken into account and a tile approach is used to compute the grid-box mean surface fluxes of mean quantities, the issue becomes more tricky. Within the framework of the tile approach, the surface grid box of an atmospheric model is divided into a number of tiles that differ in terms of various surface and soil characteristics, e.g., land-cover type and soil properties. The fluxes of scalar quantities (and of momentum) are computed for individual tiles, and the grid-box mean fluxes are then found as the weighted mean of the tile fluxes using the tile fractional areas as the weights. In the present paper, we propose the surface boundary conditions for the variances and covariances of scalar quantities that are consistent with the tile approach.

2 Transport Equations for Scalar (Co)Variances

Turbulence parametrization schemes used in atmospheric models are formulated in terms of thermodynamic variables that are approximately conserved in the condensation and evaporation processes. Herein, we use the total water specific humidity $q_t = q + q_l$ and the liquid water potential temperature $\theta_l = \theta - (\theta/T)\left(L_v/c_p\right) q_l$ as moist quasi-conservative vari-

ables. Here, q is the specific humidity (the mass of water vapour per unit mass of moist air), q_l is the liquid water specific humidity (the mass of cloud water per unit mass of moist air), θ is the potential temperature, T is the absolute temperature, L_v is the heat of vaporization, and c_p is the specific heat of air at constant pressure. In unsaturated conditions ($q_l = 0$), q_t and θ_l reduce to the dry variables q and θ, respectively. In what follows, q_t and θ_l are also referred to as simply the humidity and temperature, respectively.

Within the framework of the so-called boundary-layer approximation (where all horizontal derivatives are neglected and the grid-box mean vertical velocity is zero in the second-moment equations but not in the equations for mean fields), the transport equation for the temperature–humidity covariance reads

$$\frac{\partial}{\partial t}\langle \theta_l' q_t' \rangle + \frac{\partial}{\partial z}\langle w' \theta_l' q_t' \rangle = -\langle w' q_t' \rangle \frac{\partial \langle \theta_l \rangle}{\partial z} - \langle w' \theta_l' \rangle \frac{\partial \langle q_t \rangle}{\partial z} - 2\epsilon_{\theta q}, \tag{1}$$

where t is time, z is the height above the underlying surface, w is the vertical velocity, and $\epsilon_{\theta q}$ is the dissipation rate of $\langle \theta_l' q_t' \rangle$. The angle brackets denote (grid-box) mean quantities, and a prime denotes a fluctuation about the mean. Replacing q_t with θ_l (θ_l with q_t) in Eq. 1, we obtain the temperature-variance (humidity-variance) equation.

Within the framework of the algebraic and one-equation TKE schemes, the left-hand side (l.h.s.) of Eq. 1 is neglected. Then, parametrizing the temperature–humidity covariance dissipation rate in terms of the dissipation time scale $\tau_{\theta q}$ (which is usually set proportional to the TKE dissipation time scale), i.e., $\epsilon_{\theta q} = \langle \theta_l' q_t' \rangle / \tau_{\theta q}$, one obtains an explicit algebraic expression for $\langle \theta_l' q_t' \rangle$. If the l.h.s. of Eq. 1 is retained, a parametrization of the third-order term $\langle w' \theta_l' q_t' \rangle$ (flux of temperature–humidity covariance) is required, the simplest of which is the down-gradient diffusion formulation $\langle w' \theta_l' q_t' \rangle = -K_{\theta q} \partial \langle \theta_l' q_t' \rangle / \partial z$, where $K_{\theta q}$ is the eddy diffusivity with respect to $\langle \theta_l' q_t' \rangle$ (commonly expressed in terms of the TKE e and the turbulence time scale τ or length scale l, $K_{\theta q} \propto \tau e \propto l e^{1/2}$). If the surface grid box of an atmospheric model is treated as horizontally homogeneous, a zero third-order flux condition is appropriate,

$$\langle w' \theta_l' q_t' \rangle = 0 \qquad \text{at } z = 0, \tag{2}$$

or $-K_{\theta q} \partial \langle \theta_l' q_t' \rangle / \partial z = 0$ when the down-gradient formulation of the third-order moment is used. As stated above, Eq. 2 is compatible with the surface-layer Monin–Obukhov similarity relationships. If, however, the subgrid-scale (SGS) surface heterogeneity is taken into account, a different boundary condition is required.

3 Tile Approach

A tile approach is often used in atmospheric models to (approximately) account for the SGS heterogeneity of the underlying surface (e.g., Avissar and Pielke 1989; Moene and Dam 2014). Consider the following triple decomposition (e.g., Avissar and Chen 1993),

$$f = \langle \overline{f} \rangle + \overline{f}'' + f^s, \tag{3}$$

where f is a generic variable. As in the previous section, the angle brackets denote the quantity averaged over a grid box of a host model, an overbar denotes a mean over a tile, and a double prime denotes a fluctuation of a tile mean quantity about a grid-box mean quantity. The superscript "s" denotes a sub-tile fluctuation. By construction, $\langle \overline{f}'' \rangle = 0$ and $\overline{f^s} = 0$, i.e., the grid-box mean of the inter-tile fluctuations and the tile-mean of the sub-tile fluctuations

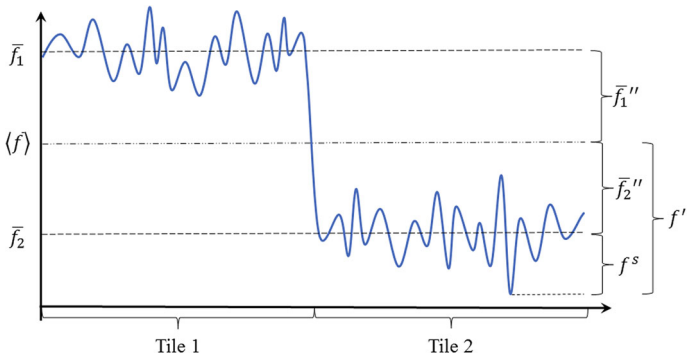

Fig. 1 A sketch illustrating triple decomposition given by Eq. 3

are zero. The relation between $\overline{f}''$, f^s and the single-primed variables f' introduced in the previous section, that is $f' = \overline{f}'' + f^s$, is illustrated in Fig. 1. Using (3), we obtain the following expression for the grid-box mean vertical flux of f,

$$\langle w' f' \rangle = \left\langle \overline{\left(\overline{w}'' + w^s\right)\left(\overline{f}'' + f^s\right)} \right\rangle = \left\langle \overline{w}'' \overline{f}'' \right\rangle + \langle \overline{w^s f^s} \rangle = \langle \overline{w^s f^s} \rangle , \tag{4}$$

where the last equality follows from the fact that $\overline{w} = 0$ at the surface. The grid-box mean vertical flux of f is the result of averaging of fluxes over individual tiles. In practice, the weighted mean is used, where the weights are equal to the fractional areas of the various tiles.

Transport equations for mean scalar quantities contain the divergence of second-order moments, i.e., fluxes of mean quantities. Likewise, transport equations for second-order moments (scalar variances and covariances) contain the divergence of third-order moments, i.e., fluxes of variances and covariances. If a tile approach is used to account for the effect of surface heterogeneity on the surface fluxes of mean scalar quantities, it is inconsistent to ignore the influence of heterogeneity on the surface fluxes of scalar (co)variances. In order to communicate the available information on the surface heterogeneity to the boundary-layer turbulence, third-order flux boundary conditions different from (2) should be used. This will increase the consistency between various components of an atmospheric model.

4 Surface Boundary Conditions Consistent with the Tile Approach

Using Eq. 3, we obtain the following expression for the triple correlation of the vertical velocity, w, and the two scalars, θ_l and q_t,

$$\begin{aligned} \langle w' \theta_l' q_t' \rangle &= \left\langle \overline{\left(\overline{w}'' + w^s\right)\left(\overline{\theta_l}'' + \theta_l^s\right)\left(\overline{q_t}'' + q_t^s\right)} \right\rangle \\ &= \left\langle \overline{w}'' \overline{\theta_l}'' \overline{q_t}'' \right\rangle + \left\langle \overline{w}'' \overline{\theta_l^s q_t^s} \right\rangle + \left\langle \overline{\theta_l}'' \overline{w^s q_t^s} \right\rangle + \left\langle \overline{q_t}'' \overline{w^s \theta_l^s} \right\rangle + \left\langle \overline{w^s \theta_l^s q_t^s} \right\rangle \\ &\equiv \left\langle \overline{w}'' \overline{\theta_l}'' \overline{q_t}'' \right\rangle + \left\langle \overline{w}'' \overline{\theta_l^s q_t^s}'' \right\rangle + \left\langle \overline{\theta_l}'' \overline{w^s q_t^s}'' \right\rangle + \left\langle \overline{q_t}'' \overline{w^s \theta_l^s}'' \right\rangle + \left\langle \overline{w^s \theta_l^s q_t^s} \right\rangle , \end{aligned} \tag{5}$$

where the second equality follows from the condition $\left\langle \overline{f}'' \right\rangle = 0$. The first two terms on the right-hand side (r.h.s.) of Eq. 5 are zero at the surface because of the zero vertical velocity

$\overline{w}$. The last term on the r.h.s. cannot be estimated if a Monin–Obukhov-type surface-layer parametrization scheme that neglects the third-order covariances is applied to individual tiles (see comment below). The third and the fourth terms on the r.h.s. of Eq. 5 are zero if the grid box of the host model is horizontally homogeneous. If the grid box is heterogeneous, the temperature $\overline{\theta_l}$ and humidity $\overline{q_t}$ differ between the tiles and so do the temperature and humidity fluxes, $\overline{w^s\theta_l^s}$ and $\overline{w^s q_t^s}$. Then, the third-order velocity–scalar covariance $\langle w'\theta_l' q_t' \rangle$, i.e., the flux of temperature–humidity covariance, is generally non-zero at the surface. The expressions for $\langle w'\theta_l'^2 \rangle$ and $\langle w' q_t'^2 \rangle$ are obtained from Eq. 5 by replacing q_t with θ_l and θ_l with q_t, respectively.

Note a close analogy between the above analysis and the analysis of Mironov and Sullivan (2016). They used large-eddy simulation (LES) to explore the second-moment budgets in the stably-stratified planetary boundary layer (PBL) over thermally homogeneous and thermally heterogeneous surfaces. Importantly, the LES-based second-moment budgets were estimated with due regard for the SGS contributions. Taking account of the SGS contributions revealed that the third-order velocity-scalar covariances are non-zero at the heterogeneous surfaces and are essential for the maintenance of second-moment budgets in the heterogeneous PBL. That finding helped explain the enhanced vertical mixing in the stably-stratified PBL over thermally heterogeneous surfaces.

Based upon the above considerations, we propose the following surface boundary conditions for the scalar variances and scalar covariance that are consistent with the tiled surface schemes,

$$\langle w'\theta_l'^2 \rangle = 2\left\langle \overline{\theta_l}''\overline{w^s\theta_l^s}'' \right\rangle, \qquad \langle w' q_t'^2 \rangle = 2\left\langle \overline{q_t}''\overline{w^s q_t^s}'' \right\rangle,$$
$$\langle w'\theta_l' q_t' \rangle = \left\langle \overline{\theta_l}''\overline{w^s q_t^s}'' \right\rangle + \left\langle \overline{q_t}''\overline{w^s\theta_l^s}'' \right\rangle. \tag{6}$$

Note that Eq. 6 reduces to the zero third-order flux boundary conditions over homogeneous surfaces, cf. Eq. 2.

We note in passing that the above considerations would make no change as to the surface boundary condition for the TKE, even though the surface may be heterogeneous. Indeed, replacing q_t and θ_l in Eq. 6 with u_i yields a zero third-order flux $\langle w' u_i'^2 \rangle$ at the surface because of no-slip surface boundary condition for the velocity $\overline{u_i} = 0$.

A comment on the fidelity of Eq. 6 is in order. As the tile approach outlined above is applied, it is tacitly assumed that the inter-tile fluctuations $\overline{f}''$ (considerably) exceed the sub-tile fluctuations f^s. If $\overline{f}'' \gg f^s$, the members of Eq. 6 account for a major part of the surface heterogeneity. There are surface types, however, whose heterogeneity is very difficult, if possible at all, to describe by means of the conventional tile approach. Examples are forest canopies with their small-scale, very complex structure. For such surfaces, the last term on the r.h.s. of Eq. 5 is large and should not be neglected. A surface-layer parametrization scheme is then required that is capable of estimating the third-order velocity–scalar covariances. This basic problem is beyond the scope of the present study whose aim is to reconcile the treatment of the third-order and the second-order fluxes within the framework of the conventional tile approach.

The surface boundary conditions given by Eq. 6 provide an intimate coupling of the scalar variances and covariance with many other quantities characterizing the atmosphere and the soil. In order to illustrate this coupling, consider the moisture and heat balance equations at the underlying surface for individual tiles. The moisture balance equation reads

$$\overline{P\,P} + \rho\overline{w^s q_t^s} = \overline{G_q} + \overline{Q}, \tag{7}$$

where ρ is the density, G_q is the ground moisture flux at the surface, Q is the surface run-off, and PP denotes the sum of all forms of precipitation, including (relatively slow) sedimentation of water droplets and ice crystals. Subtracting from Eq. 7 its horizontal mean, multiplying the result with $\overline{q_t}''$, and averaging horizontally, we obtain

$$\left\langle \overline{q_t}'' \overline{w^s q_t^s}'' \right\rangle = \rho^{-1} \left[\left\langle \overline{q_t}'' \overline{G_q}'' \right\rangle + \left\langle \overline{q_t}'' \overline{Q}'' \right\rangle - \left\langle \overline{q_t}'' \overline{PP}'' \right\rangle \right]. \tag{8}$$

The first two terms in brackets on the r.h.s. of Eq. 8 are generally non-zero. Over heterogeneous surfaces, the total water content, the ground moisture flux and the surface run-off vary between the tiles because of the difference in soil and/or vegetation properties. Then, the fluctuations of the ground moisture flux and of the surface run-off are likely correlated with the fluctuations of the total water content. As to the third term on the r.h.s., there is no good reason to assume that rain, snow, or hail falls differently onto some tiles than onto the others. However, if the term PP includes sedimentation of water droplets and ice crystals from fog layers and there is fog over some tiles but not over the other tiles, then $\overline{PP}''$ and the covariance $\left\langle \overline{q_t}'' \overline{PP}'' \right\rangle$ may appear to be different from zero. Rain or snow falling through the fog layers may amplify the influence of fog via the seeder-feeder effect (e.g., Houze 1993, and references therein).

Consideration of the heat balance of the underlying surface,

$$\overline{R_s} + \overline{R_l} + \rho c_p \overline{w^s \theta_l^s} + \rho L_v \overline{w^s q_t^s} = \overline{G_\theta}, \tag{9}$$

yields the following expression,

$$\begin{aligned} \left\langle \overline{\theta_l}'' \overline{w^s \theta_l^s}'' \right\rangle = (\rho c_p)^{-1} \Big[& \left\langle \overline{\theta_l}'' \overline{G_\theta}'' \right\rangle - \left\langle \overline{\theta_l}'' \overline{R_s}'' \right\rangle - \left\langle \overline{\theta_l}'' \overline{R_l}'' \right\rangle \\ & - L_v \left(\left\langle \overline{\theta_l}'' \overline{G_q}'' \right\rangle + \left\langle \overline{\theta_l}'' \overline{Q}'' \right\rangle - \left\langle \overline{\theta_l}'' \overline{PP}'' \right\rangle \right) \Big]. \end{aligned} \tag{10}$$

Here, G_θ is the ground heat flux at the surface, and R_s and R_l are, respectively, the solar radiation balance and the longwave radiation balance at the surface. The first three terms on the r.h.s. of Eq. 10 are generally non-zero. The solar radiation balance varies between the tiles because of the difference in the tile albedo, and the longwave radiation balance and the ground heat flux vary because of the difference in temperature between the tiles. The fourth term may also be appreciable if the surface temperature and humidity are correlated (the ground moisture flux is to a large extent determined by the surface humidity). The magnitude of the last two terms on the r.h.s. of Eq. 10, namely, the correlations of the surface temperature with the run-off and with the precipitation flux, is difficult to estimate a priori. These correlations are presumably small.

For the flux of the temperature–humidity covariance, the following expression holds,

$$\begin{aligned} \left\langle \overline{\theta_l}'' \overline{w^s q_t^s}'' \right\rangle + \left\langle \overline{q_t}'' \overline{w^s \theta_l^s}'' \right\rangle = (\rho c_p)^{-1} & \left[\left\langle \overline{q_t}'' \overline{G_\theta}'' \right\rangle - \left\langle \overline{q_t}'' \overline{R_s}'' \right\rangle - \left\langle \overline{q_t}'' \overline{R_l}'' \right\rangle \right] \\ + \rho^{-1} & \Big[\left\langle \overline{\theta_l}'' \overline{G_q}'' \right\rangle + \left\langle \overline{\theta_l}'' \overline{Q}'' \right\rangle - \left\langle \overline{\theta_l}'' \overline{PP}'' \right\rangle \\ - \frac{L_v}{c_p} & \left(\left\langle \overline{q_t}'' \overline{G_q}'' \right\rangle + \left\langle \overline{q_t}'' \overline{Q}'' \right\rangle - \left\langle \overline{q_t}'' \overline{PP}'' \right\rangle \right) \Big], \end{aligned} \tag{11}$$

where a number of terms on the r.h.s. of Eq. 11 are generally non-zero over heterogeneous surfaces for similar reasons as discussed above.

It should be realized that, although the boundary conditions given by Eq. 6 look like the flux boundary conditions, this is not the case. The point is that the surface fluxes $\overline{w^s \theta_l^s}$ and $\overline{w^s q_t^s}$ are not merely "prescribed" but are determined jointly with the temperature and moisture profiles within the soil (and hence with the surface temperature and moisture). The coupling

of the soil and the atmosphere is provided by the surface balance equations for heat, Eq. 9, and moisture, Eq. 7. The surface boundary conditions given by Eqs. 6, 8, 10 and 11 are, in fact, the so-called Robin boundary conditions, also known as the impedance boundary conditions, or convective boundary conditions. The Robin boundary condition is a weighted combination of Dirichlet and Neumann boundary conditions that relates the quantity in question and its derivative normal to the boundary. This may be written symbolically as

$$AX + B\frac{\partial X}{\partial z} = C. \tag{12}$$

By way of illustration consider Eq. 10, in which case $X = \left\langle \overline{\theta_l}''^2 \right\rangle$. Using the first member of Eq. 6 and invoking the down-gradient diffusion formulation,

$$2\left\langle \overline{\theta_l}'' \overline{w^s \theta_l^s}'' \right\rangle = \left\langle w' \theta_l'^2 \right\rangle = -K_{\theta\theta} \frac{\left\langle \overline{\theta_l}''^2 \right\rangle}{\partial z}, \tag{13}$$

we obtain $B = -\frac{1}{2} K_{\theta\theta}$ ($K_{\theta\theta}$ being the eddy diffusivity with respect to the temperature variance). The surface longwave radiation balance R_l is the sum of the downward longwave radiation flux from the atmosphere F_a and the upward longwave radiation flux from the surface $\epsilon\sigma T^4$, where ϵ is the surface emissivity, and σ is the Stefan-Boltzmann constant. Linearizing T^4 about the grid-box mean temperature, neglecting sub-tile fluctuations, using the definition of the liquid water potential temperature to express T through θ_l and q_l, and neglecting the pressure fluctuations (this assumption yields $T/\theta = \langle \overline{T} \rangle / \langle \overline{\theta} \rangle$), we obtain the following expression for the fluctuation of the tile-mean longwave radiation balance about its grid-box mean value,

$$\overline{R_l} - \langle \overline{R_l} \rangle \equiv \overline{R_l}'' = \overline{F_a}'' + \epsilon\sigma \langle \overline{T} \rangle^3 \left(\frac{L_v}{c_p} \overline{q_l}'' + \frac{\langle \overline{T} \rangle}{\langle \overline{\theta} \rangle} \overline{\theta_l}'' \right). \tag{14}$$

Multiplying Eq. 14 by $\overline{\theta_l}''$ and averaging, we obtain

$$\left\langle \overline{\theta_l}'' \overline{R_l}'' \right\rangle = \left\langle \overline{\theta_l}'' \overline{F_a}'' \right\rangle + \epsilon\sigma \langle \overline{T} \rangle^3 \left(\frac{L_v}{c_p} \left\langle \overline{\theta_l}'' \overline{q_l}'' \right\rangle + \frac{\langle \overline{T} \rangle}{\langle \overline{\theta} \rangle} \left\langle \overline{\theta_l}''^2 \right\rangle \right), \tag{15}$$

where it can be seen that $\left\langle \overline{\theta_l}'' \overline{R_l}'' \right\rangle$ contributes to A and C in Eq. 12. Since the ground heat flux G_θ depends on the surface temperature, the correlation $\left\langle \overline{\theta_l}'' \overline{G_\theta}'' \right\rangle$ also contributes to A, and may also contribute to C, e.g., due to inter-tile variations of the soil temperature conductivity. The shortwave radiation balance R_s, the ground moisture flux G_q, the run-off Q, and the precipitation flux PP do not explicitly depend on the surface temperature, so the correlations of their inter-tile fluctuations with $\overline{\theta_l}''$ do not contain $\left\langle \overline{\theta_l}''^2 \right\rangle$. Hence, $\left\langle \overline{\theta_l}'' \overline{R_s}'' \right\rangle$, $\left\langle \overline{\theta_l}'' \overline{G_q}'' \right\rangle$, $\left\langle \overline{\theta_l}'' \overline{Q}'' \right\rangle$ and $\left\langle \overline{\theta_l}'' \overline{PP}'' \right\rangle$ contribute to C. In summary, each of the three coefficients in Eq. 12 is different from zero, suggesting that the surface boundary condition for the temperature variance given by Eqs. 6 and 10 is indeed the Robin boundary condition.

Note finally that, in practice, either the l.h.s. or the r.h.s. of Eq. 10 can be used to specify (compute) the boundary condition for the temperature variance (similarly for the humidity variance, Eq. 8, and for the temperature–humidity covariance, Eq. 11). The choice depends on the numerical approximation scheme used in the atmospheric model in question, the degree of its implicitness, numerical stability of solutions, and the model code architecture.

5 Single-Column Numerical Experiment

In order to illustrate the impact of the surface boundary conditions for the scalar (co)variances on the boundary-layer structure and mixing intensity, a single-column numerical experiment is performed. An idealized, dry, stably-stratified PBL set-up is used. The TKE – Scalar Variances (TKESV) turbulence parametrization scheme (Mironov and Machulskaya 2017) is used to describe the vertical mixing in the boundary layer. The underlying surface of the column is divided into two tiles with different prescribed surface temperatures. Turbulent fluxes of sensible heat and momentum at the surface are computed individually for each tile using the Monin–Obukhov flux-profile relationships (e.g., Dyer 1974), and the tile-specific fluxes are then averaged to provide the surface boundary conditions for the mean potential temperature and mean wind velocity. The two tiles have equal relative weights of 1/2. For the potential temperature variance, the Neumann boundary condition at the underlying surface is used, see Eq. 13. The temperature-variance flux $\left\langle w'\theta_l'^2 \right\rangle$ is either set to zero (the effect of surface heterogeneity on the temperature variance is ignored), or is computed using the first member of Eq. 6 (the effect of surface heterogeneity is accounted for).

The following governing parameters are used in our numerical experiment (cf. Beare et al. 2006; Stoll and Porté-Agel 2009; Mironov and Sullivan 2016). The Coriolis parameter is $f_c = 1.39 \times 10^{-4}\ s^{-1}$, the buoyancy parameter $\beta = g/\theta_r$ is constant, with the acceleration due to gravity $g = 9.81\ \mathrm{m^2\ s^{-1}}$ and the reference temperature $\theta_r = 265$ K. A constant aerodynamic roughness length of $z_0 = 0.1$ m is utilized for both temperature and velocity. The flow is driven by a constant streamwise geostrophic velocity component $U_g = 8\ \mathrm{m\ s^{-1}}$ (the spanwise geostrophic velocity component is zero). The initial temperature profile consists of a mixed layer of depth 100 m and a height-constant potential temperature of 265 K and a stably-stratified layer above, where potential temperature increases linearly at a rate of $0.01\ \mathrm{K\ m^{-1}}$. The initial streamwise velocity component increases linearly from zero at the surface to U_g at the mixed-layer top and is equal to U_g aloft. The initial spanwise velocity component is zero. Both surface tiles are initialized with the same temperature equal to the initial temperature of the mixed layer. Then, the temperature of one tile is kept constant in time, whereas the other tile is cooled at a rate of $-1.5\ \mathrm{K\ h^{-1}}$ over eight hours. Following the 8-h cooling period, the runs are continued over two more hours, keeping the temperature of both tiles constant in time. The results presented below are obtained by means of averaging over the last two hours of simulations.

Figure 2 shows vertical profiles of potential-temperature variance, vertical potential-temperature flux, TKE, and mean potential temperature from the runs with zero and non-zero surface flux of the temperature variance. As seen from Fig. 2a, the temperature variance in the run with non-zero third-order flux is larger in the lower part of the PBL as compared to the run with zero flux. In the present simulations, the buoyancy stratification in the surface layer is stable over the "cold" tile, but proves to be slightly convective over the "warm" tile. The surface layer remains stably stratified in the average (mean over the two tiles) sense. Over the cold tile, where $\overline{\theta}'' < 0$, the surface temperature flux is more negative than the mean flux, hence $\overline{w^s\theta^s}'' < 0$, while over the warm tile, where $\overline{\theta}'' > 0$, the surface temperature flux is larger than the mean flux, $\overline{w^s\theta^s}'' > 0$. As a result, $\overline{\theta}$ and $\overline{w^s\theta^s}$ are positively correlated, leading to a positive (directed upward) third-order flux of the temperature variance. This is illustrated schematically in Fig. 3. Note that the surface layer over the warm tile may be convective (as in our simulations), neutral, or even stable; the last possibility is shown in Fig. 3 with the dashed line. An important point is that the flux $\overline{w^s\theta^s}$ over the warm tile is less negative than over the cold tile (the opposite case can also be encountered

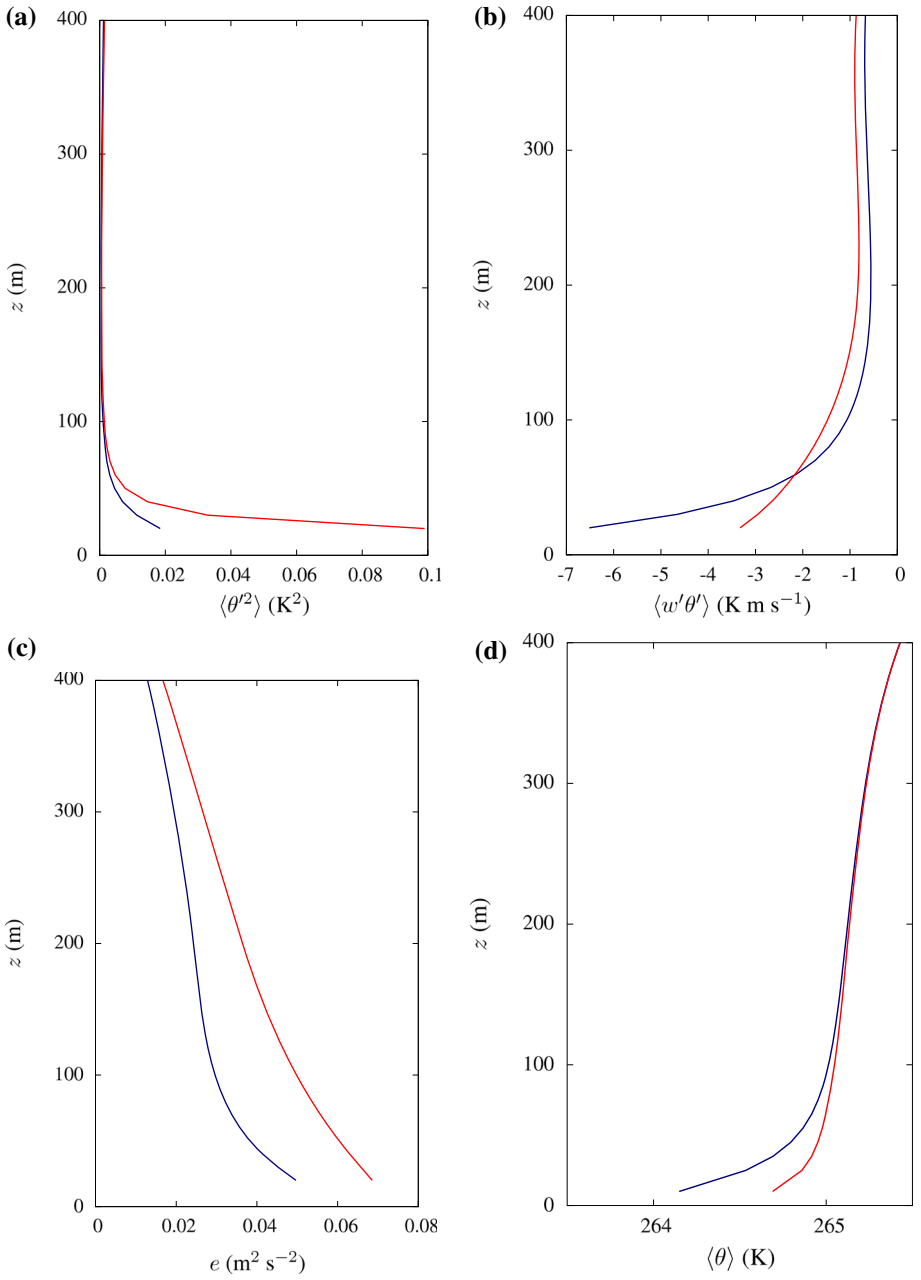

Fig. 2 Vertical profiles of **a** potential-temperature variance, **b** vertical potential-temperature flux, **c** TKE (e) and **d** mean potential temperature from the runs with the zero flux of the temperature variance at the surface (blue curves) and with the temperature-variance flux computed from the first member of Eq. 6 (red curves). Shown are the values from the first model level upwards

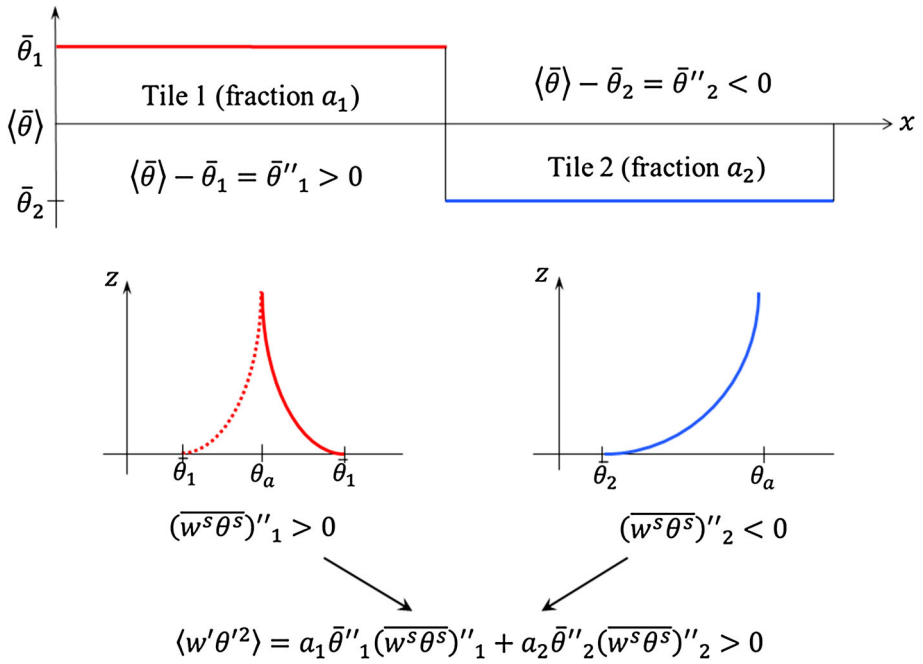

Fig. 3 A sketch illustrating the application of the surface boundary condition for the temperature variance given by the first member of Eq. 6

as briefly discussed below). A positive temperature-variance flux in the run using a non-zero temperature-variance flux computed from the first member of Eq. 6 leads to an increased temperature variance near the surface as compared to the run with zero temperature-variance flux.

An increase of the temperature variance in the run with non-zero third-order flux explains the results shown in Fig. 2b–d (the chain of arguments is the same as in Mironov and Sullivan 2016). Consideration of the temperature-flux budget in stably stratified flows suggests that a downward (negative) temperature flux is generated by the mean-gradient term. The buoyancy term, represented by the temperature variance times the buoyancy parameter, generates an upward (positive) temperature flux that partially compensates the downward flux. As the temperature variance increases, the resulting temperature flux becomes less negative; this is clearly seen in Fig. 2b. In a stably stratified flow, the buoyancy flux, i.e., the temperature flux times the buoyancy parameter, is the sink term in the TKE budget. A reduced magnitude of the buoyancy flux results in an increased TKE, Fig. 2c, which in turn leads to an enhanced vertical mixing and in a more vertically homogeneous boundary-layer temperature, Fig. 2d.

It should be pointed out that Eq. 6 does not necessarily yield a positive (upward) temperature-variance flux as schematized in Fig. 3. A negative (downward) temperature-variance flux is also possible, a situation that may be encountered in strongly stable surface layer. In a weakly or moderately stable flow, an increase of the temperature gradient in the surface layer results in an increased magnitude of the surface temperature flux (the flux becomes more negative), since the static stability is not large enough to significantly reduce the vertical turbulent heat transfer. In a strongly stable surface layer, turbulence is so powerfully suppressed by the buoyancy forces that an increase in the temperature gradient results in

a reduced magnitude of the surface temperature flux. As a result, $\overline{\theta}'' < 0$ and $\overline{w^s\theta^s}'' > 0$ (the temperature flux is less negative) over a cold tile, and $\overline{\theta}'' > 0$ and $\overline{w^s\theta^s}'' < 0$ (the temperature flux is more negative) over a warm tile. Then, $\overline{\theta}$ and $\overline{w^s\theta^s}$ are negatively correlated, leading to a negative (downward) third-order flux of the temperature variance at the surface.

Numerical experiment discussed above shows an appreciable effect of the surface boundary conditions for the temperature variance on the PBL structure and mixing intensity. Results from other numerical experiments (not shown) suggest that in many situations the effect is small or even negligible. It should be stressed that this fact cannot be the reason for not using Eq. 6 to specify the boundary conditions for the scalar (co)variances that are in harmony with the tile approach. Whether the effect of non-zero surface fluxes of scalar (co)variances is substantial or not is difficult to say a priori, let alone an increased overall consistency of an atmospheric model that makes use of Eq. 6.

6 Conclusions

The problem of boundary conditions for the variances and covariances of scalar quantities at the underlying surface is considered. Boundary conditions are proposed that are consistent with the tile approach used to compute fluxes of scalar quantities (liquid water potential temperature and total water specific humidity) over heterogeneous surfaces. The proposed surface boundary conditions provide an intimate coupling of the scalar (co)variances with many other quantities characterizing the atmosphere and the soil, such as the spatially-heterogeneous ground fluxes of heat and moisture and the surface radiation balance. It is shown that the proposed conditions are the so-called Robin boundary conditions, also known as the impedance boundary conditions, or convective boundary conditions. The Robin boundary conditions are weighted combinations of Dirichlet and Neumann boundary conditions that relate the quantity in question (e.g., temperature variance) and its derivative normal to the boundary. The effect of the proposed boundary conditions on mixing in an archetypical, dry, stably-stratified PBL is illustrated with a single-column numerical experiment.

The proposed boundary conditions should be applied in atmospheric models utilizing the tile approach and turbulence parametrization schemes that carry transport equations for scalar (co)variances with due regard to the third-order transport (diffusion) terms. The use of Eq. 6 instead of simply setting the third-order scalar (co)variance fluxes at the surface to zero makes the entire atmospheric model more consistent. The associated computational burden is negligible. The proposed boundary conditions for scalar (co)variances are implemented into the test version of the NWP model COSMO that utilizes the TKESV turbulence parametrization scheme (Mironov and Machulskaya 2017).

Acknowledgements The authors are grateful to three anonymous reviewers whose comments helped to improve the manuscript.

References

Avissar R, Chen F (1993) Development and analysis of prognostic equations for mesoscale kinetic energy and mesoscale (subgrid scale) fluxes for large-scale atmospheric models. J Atmos Sci 50:3751–3774

Avissar R, Pielke RA (1989) A parameterization of heterogeneous land surfaces for atmospheric numerical models and its impact on regional meteorology. Mon Weather Rev 117:2113–2136

Beare RJ, Macvean MK, Holtslag AAM, Cuxart J, Esau I, Golaz JC, Jimenez MA, Khairoutdinov M, Kosovic B, Lewellen D, Lund TS, Lundquist JK, McCabe A, Moene AF, Noh Y, Raasch S, Sullivan PP (2006) An intercomparison of large-eddy simulations of the stable boundary layer. Boundary-Layer Meteorol 118:242–272

Dyer AJ (1974) A review of flux-profile relationships. Boundary-Layer Meteorol 7:363–372

Houze RA (1993) Cloud dynamics. Academic Press, New York

Kenjereš S, Hanjalić K (2002) Combined effects of terrain orography and thermal stratification on pollutant dispersion in a town valley: a T-RANS simulation. J Turbul 3:1–25

Lynn BH, Rind D, Avissar R (1995) The importance of mesoscale circulations generated by subgrid-scale landscape heterogeneities in general circulations models. J Clim 8:191–205

Machulskaya E, Mironov D (2013) Implementation of TKE-scalar variance mixing scheme into COSMO. COSMO Newsl 13:25–33

Mellor GL, Yamada T (1974) A hierarchy of turbulence closure models for planetary boundary layers. J Atmos Sci 31:1791–1806

Mironov DV (2009) Turbulence in the lower troposphere: second-order closure and mass-flux modelling frameworks. In: Hillebrandt W, Kupka F (eds) Interdisciplinary aspects of turbulence, Lect. Notes Phys., vol 756, Springer, pp 161–221

Mironov DV, Machulskaya EE (2017) A turbulence kinetic energy—scalar variance turbulence parameterization scheme. COSMO Technical Report 30, available from http://www.cosmo-model.org

Mironov DV, Sullivan PP (2016) Second-moment budgets and mixing intensity in the stably stratified atmospheric boundary layer over thermally heterogeneous surfaces. J Atmos Sci 73:449–464

Moene AF, van Dam JC (2014) Transport in the atmosphere-vegetation-soil continuum. Cambridge University Press, Cambridge

Nakanishi M, Niino H (2004) An improved Mellor–Yamada level-3 model with condensation physics: its design and verification. Boundary-Layer Meteorol 112:1–31

Stoll R, Porté-Agel F (2009) Surface heterogeneity effects on regional-scale fluxes in stable boundary layers: surface temperature transitions. J Atmos Sci 66:412–431